ADVANCED MATERIALS

Supporting Information

for *Adv. Mater.*, DOI: 10.1002/adma.201701475

Giant Ferroelectric Polarization in Ultrathin Ferroelectrics via Boundary-Condition Engineering

*Lin Xie, Linze Li, Colin A. Heikes, Yi Zhang, Zijian Hong, Peng Gao, Christopher T. Nelson, Fei Xue, Emmanouil Kioupakis, Longqing Chen, Darrel G. Schlom, Peng Wang, and Xiaoqing Pan**

Supporting Information

Giant Ferroelectric Polarization in Ultrathin Ferroelectrics via Boundary-condition Engineering

*Lin Xie, Linze Li, Colin A. Heikes, Yi Zhang, Zijian Hong, Peng Gao, Christopher T. Nelson, Xue Fei, Emmanouil Kioupakis, Longqing Chen, Darrel G. Schlom, Peng Wang, Xiaoqing Pan**

1. Polar displacement mapping

Atomic polar displacements $\mathbf{D}_{FB}$ were directly measured from the STEM HAADF image by fitting the image with a series of two-dimensional (2D) Gaussian functions[S1]. After fitting, the atomic positions are extracted from the centers of these 2D Gaussian functions. $\mathbf{D}_{FB}$ is defined as the off-center displacement of the central *B*-site Fe atoms with respect to the center of four surrounding *A*-site Bi atoms. It is well accepted that the polarization of BFO is essentially due to the relative displacements between Bi and O atoms[S2]. Hence the relative displacement between Fe and Bi, $\mathbf{D}_{FB}$, is in the opposite direction of the actual polarization and its value is proportional to the polarization.

2. Atomic structure of Bi_2O_3

Figure S1a displays the schematic atomic structure of Bi_2O_3[25]. The lattice parameters of Bi_2O_3 are $a=b=7.7439$ Å, $c=5.6287$ Å, $\alpha=\beta=\gamma=90°$, respectively. It can be readily found that the lattice of Bi_2O_3 is compatible with $TbScO_3$'s $[110]_O \times [001]_O$ basis (~7.918 Å). **Figure S1b** displays the projected atomic structure of Bi_2O_3 viewed along [110] zone axis and the zigzag structure of Bi atoms on [001] plane can be clearly observed. This zigzag structure is in good

agreement with the experiment observations (Figure 1b) and DFT calculation results (Figure 4a).

3. Detailed studies of surface monolayers in 2 nm/5 nm/20 nm $BiFeO_3/TbScO_3$ $(1\bar{1}0)_O$ films

The ultrathin 2 nm film was characterized along the $[010]_{PC}$ direction and **Figure S2** shows the STEM HAADF image. Similar to the surface monolayer structure observed along $[100]_{PC}$ direction (Figure 1b), characteristic discontinuous surface monolayer could also be identified along the orthogonal $[010]_{PC}$ direction. Combining the structural information from these two orthogonal directions, it is suggested that these monolayers are actually discontinuously distributed on the film's surface, forming two-dimensional islands.

To gain a further understanding of the surface structure, STEM HAADF image simulation was carried out using our home-made multislice image simulation package. The atomic model for simulation was directly taken from the relaxed structure by DFT calculation and the occupancies of surface Bi_2O_3 monolayer are fixed to 50%. The parameters for the STEM imaging conditions are V=300 kV, C_3=10 nm, Δf=Scherzer defocus, C_C=1.5 mm, ΔE=0.7 eV with a convergence angle of 22 mrad. The sample thickness for simulation is 16 nm. Surface thermal-vibrations induced thermal diffuse scatterings were accounted for by specifying different Debye-Waller factors for the atoms on each different site. For BFO film, their Debye-Waller factors were taken from empirical functions (B_{Bi}=1.169, B_{Fe}=0.3106, B_O=0.7875) according to Ref. [S3]. For the Bi atoms on the surface and the subsurface, their Debye-Waller factors were set to 1.636 and 1.403, about 40% and 20% increase with respect to that of the bulk. We note that the exact values of Debye-Waller factors for the surface atoms and even for the whole structure are somewhat arbitrarary because they depend on a number of factors, for example, crystal structure and bond strength. Thus our simulation only

offers a qualitative understanding of the structure. **Figure S3** displays the simulated results without and with thermal diffuse scatterings, respectively. For a better comparison, the simulated image intensity I is normalized by its maximum and minimum as:

$$I_{\text{norm}} = \frac{I}{I_{\text{max}} - I_{\text{min}}} \tag{S1}$$

As is shown in **Figure S3a** and **S3d**, the contrast of the surface monolayer is considerably lower than that of the subsurface and the inner BiO layers due to its relatively lower atomic densities. If thermal diffuse scattering is taken into consideration, the contrast of the surface monolayer is further reduced due to a weaker channeling of electrons along the atomic columns on the surface. These results are qualitatively in agreement with our experimental findings, suggesting a formation of two-dimensional island-like monolayer structures on BFO film.

In order to testify the hypothese that the surface monolayer is probably a transient state during growth, a sequence of BFO/TSO films with thicknesses of 5 nm and 20 nm were grown and their structure were characterized by atomic-resolution STEM HAADF imaging as well. As are shown in **Figure S4** and **Figure S5**, the characteristic single atomic layer can be clearly observed on the surface of the 5 nm and 20 nm films (indicated by yellow arrows in **Figure S4a** and **S5b**), implying that these surface monolayers are ubiquitous in BFO films and might act as nucleation sites during the growth. If more FeO_2 is added, these peculiar surface structures would absorb FeO_2 and transit into proper BFO layers. In analogue to the ultrathin 2 nm thick film, $-\mathbf{D}_{\text{FB}}$, $-D_{\text{FB}}^{(z)}$ and c/a ratio are measured for the 5 nm thick film and the results are given in **Figure S4b-S4e**. Although the domain structure of the 5 nm thick film is of the conventional 109° domain configuration for *R*-phase BFO, its ferroelectricity in the vicinity of the surface is substantially affected by the surface layers. As shown in Figure S4b and S4e, $-D_{\text{FB}}^{(z)}$ increases rapidly in the vicinity of the surface and reaches about ~0.48 Å at the top surface. Meanwhile, a substantial increase of c/a ratio is also discovered. These

findings are identical to those for the 2 nm thick film. Similar surface structure can also be identified in the 20 nm thick film. **Figure S5a** shows the dark-field image of the 20 nm film and the corresponding atomic-resolution STEM HAADF image is given in **Figure S5b**, in which the same surface structure can also be found (as indicated by yellow arrows). The polarization in the middle of the 20 nm thick film are mapped and the results are given in **Figure S5c**, where polarization is mainly along $<111>_{PC}$ directions and domains are separated by a 109° domain wall.

4. DFT calculation of ultrathin $BiFeO_3$ film with surface Bi_2O_3

DFT calculations were carried out using Vienna Ab-initio Software Package (VASP)[S4] within the framework of PAW[S5,S6] and LSDA+U[S7]. A symmetrical slab consisting of 5 layers of BiO planes and 5 layers of FeO_2 planes was built on top of 6 unit cells of $TbScO_3$ $(1\bar{1}0)_O$. The supercell was chosen to be $\sqrt{2}\times\sqrt{2}$ of the perovskite pseudocubic unit cell and the in-plane lattice constant was fixed to the experimental value of TSO (a=5.47 Å, b=5.73 Å). The k-points were sampled using a 5×5×1 Monkhorst-Pack mesh[S8], the planewave cut-off energy set to 500 eV and U and J parameters were chosen as U_{eff}=U-J=2 eV[S2]. To avoid spurious electric fields due to the slab configuration, a 15 Å vacuum region was used to separate the periodic slabs, and the dipole correction was turned on during the calculation. A larger vacuum separation of 20 Å was tested as well and the total energy difference was only ~1 meV. The system is first relaxed by the force criterion (<0.005 eV/Å), which reproduces the rhombohedral ferroelectric phase and G-type antiferromagnetic ground state of BFO. After the structure relaxation, a stoichiometric single atomic Bi_2O_3 layer was added on top of the relaxed BFO slab and further relaxations were performed until the maximum force is <0.005 eV/Å. The relaxed structure is insulating.

The Born effective charges (BEC) were calculated by finite difference of Berry-phase polarizations[S9,S10]. The calculated BECs are +4.56, +3.3 and -2.62 for Bi, Fe and O atoms, respectively.

5. Phase-field simulations

In the phase-field simulations, two sets of order parameters are considered, namely spontaneous polarization P_i (i=1, 2, 3) and spontaneous oxygen octahedral rotation θ_i (i=1, 2, 3). The evolution of order parameters are governed by the time-dependent Ginzburg-Landau (TDGL) equations:

$$\frac{\partial P_i(\vec{r},t)}{\partial t} = -L_1 \frac{\delta F}{\delta P_i(\vec{r},t)} \quad (i=1, 2, 3) \tag{S2}$$

$$\frac{\partial \theta_i(\vec{r},t)}{\partial t} = -L_2 \frac{\delta F}{\delta \theta_i(\vec{r},t)} \quad (i=1, 2, 3) \tag{S3}$$

where $\vec{r}$ is the spatial position vector, t is the evolution time step, L_1 and L_2 are the kinetic coefficients for polarization and octahedral rotation, respectively. F is the free energy of the system which is the volume integration of Landau, elastic, electric and gradient energy densities:

$$F = \int \left(f_{\text{Landau}} + f_{\text{elastic}} + f_{\text{electric}} + f_{\text{gradient}} \right) \mathrm{d}V \tag{S4}$$

The bulk Landau energy density has the contribution from polarization and octahedral rotation, namely:

$$f_{\text{Landau}} = f_{\text{polarization}} + f_{\text{rotation}} \tag{S5}$$

Detailed expressions of the energy density as well as method of solving the phase-field equations can be found in literatures[S11–S14]. All the parameters are taken from literatures[S14,S15]. A quasi-2D simulation with system size of $64\Delta x \times 4\Delta y \times 25\Delta z$ is performed. The grid spacing is chosen as 0.4 nm, i.e., $\Delta x = \Delta y = \Delta z = 0.4$ nm. The system consists of 10 grids

of substrate layer, 5 grids of $BiFeO_3$ and 10 grids of air from the bottom to the top along the thickness direction. Mixed electric boundary condition is used, where the dielectric displacement is zero at the bottom of the film and fixed electric potential at the film top. A bias of -1.3V is added at specific location on top of the film to simulate the effective polarizing field induced by the Bi_2O_3 layer[S16], whereas the bias at all the other top areas are fixed to zero to account for the charge compensation from air. Periodic boundary condition is assumed along the in-plane dimensions (*x* and *y* dimensions), while a superposition spectral method is used along *z* direction[S13]. Besides the above structure, in order to accurately treat the open-circuit boundary condition, that is, without charge compensation at the surface, a structure model without surface layers was also calculated in the phase-field simulation.

References

[S1] C. T. Nelson, B. Winchester, Y. Zhang, S.-J. Kim, A. Melville, C. Adamo, C. M. Folkman, S.-H. Baek, C.-B. Eom, D. G. Schlom, L.-Q. Chen, X. Pan, *Nano Lett.* **2011**, *11*, 828.
[S2] J. B. Neaton, C. Ederer, U. V. Waghmare, N. A. Spaldin, K. M. Rabe, *Phys. Rev. B* **2005**, *71*, 014113.
[S3] L. M. Peng, G. Ren, S. L. Dudarev, M. J. Whelan, *Acta Cryst. A* **1996**, *52*, 456.
[S4] G. Kresse, J. Furthmüller, *Phys. Rev. B* **1996**, *54*, 11169.
[S5] P. E. Blöchl, *Phys. Rev. B* **1994**, *50*, 17953.
[S6] G. Kresse, D. Joubert, *Phys. Rev. B* **1999**, *59*, 1758.
[S7] S. L. Dudarev, G. A. Botton, S. Y. Savrasov, C. J. Humphreys, A. P. Sutton, *Phys. Rev. B* **1998**, *57*, 1505.
[S8] H. J. Monkhorst, J. D. Pack, *Phys. Rev. B* **1976**, *13*, 5188.
[S9] R. D. King-Smith, D. Vanderbilt, *Phys. Rev. B* **1993**, *47*, 1651.
[S10] R. D. King-Smith, D. Vanderbilt, *Phys. Rev. B* **1994**, *49*, 5828.
[S11] Y. Li, S. Hu, Z. Liu, L. Chen, *Acta Mater.* **2002**, *50*, 395.
[S12] Y. L. Li, S. Y. Hu, Z. K. Liu, L. Q. Chen, *Appl. Phys. Lett.* **2002**, *81*, 427.
[S13] L. Chen, J. Shen, *Comput. Phys. Commun.* **1998**, *108*, 147.
[S14] F. Xue, Y. Gu, L. Liang, Y. Wang, L.-Q. Chen, *Phys. Rev. B* **2014**, *90*, 220101.
[S15] Q. Li, Y. Cao, P. Yu, R. K. Vasudevan, N. Laanait, A. Tselev, F. Xue, L. Q. Chen, P. Maksymovych, S. V. Kalinin, N. Balke, *Nat. Commun.* **2015**, *6*, 8985.
[S16] Q. Miao, M. Zeng, Z. Zhang, X. Lu, J. Dai, X. Gao, J.-M. Liu, *Appl. Phys. Lett.* **2014**, *104*, 182903.

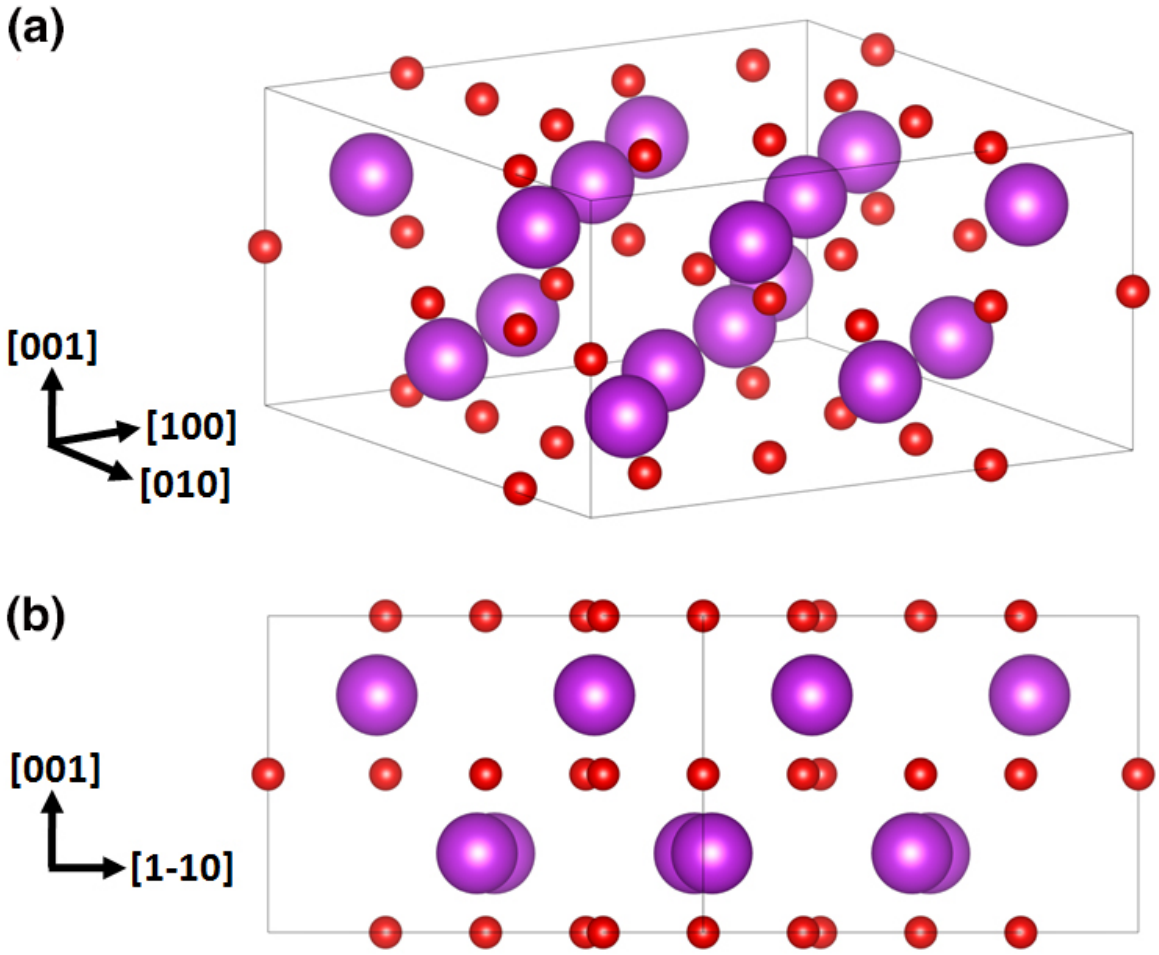

Figure S1. Schematic structure of Bi_2O_3. a) Atomic structure of Bi_2O_3 and b) projection view of Bi_2O_3 along [110] direction. For each Bi_2O_3 atomic layer, its structure has a good match of the BiO plane of $BiFeO_3$ and the stacking of a single Bi_2O_3 layer on BiO plane is similar to a natural stacking of Bi_2O_3 layers along [001] direction.

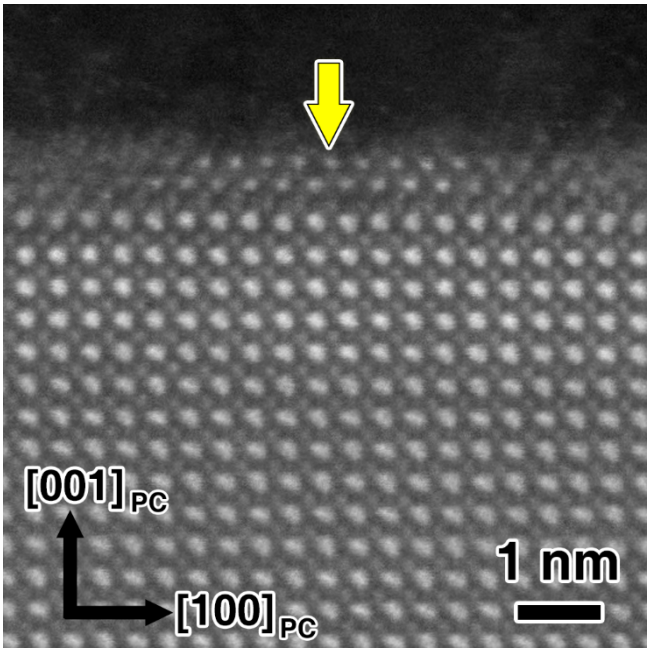

Figure S2. STEM HAADF image of a 2 nm thick $BiFeO_3/TbScO3$ $(1\bar{1}0)_O$ film viewed along the orthogonal $[010]_{PC}$ direction. The surface Bi_2O_{3-x} monolayer can be clearly seen and is indicated by the yellow arrow.

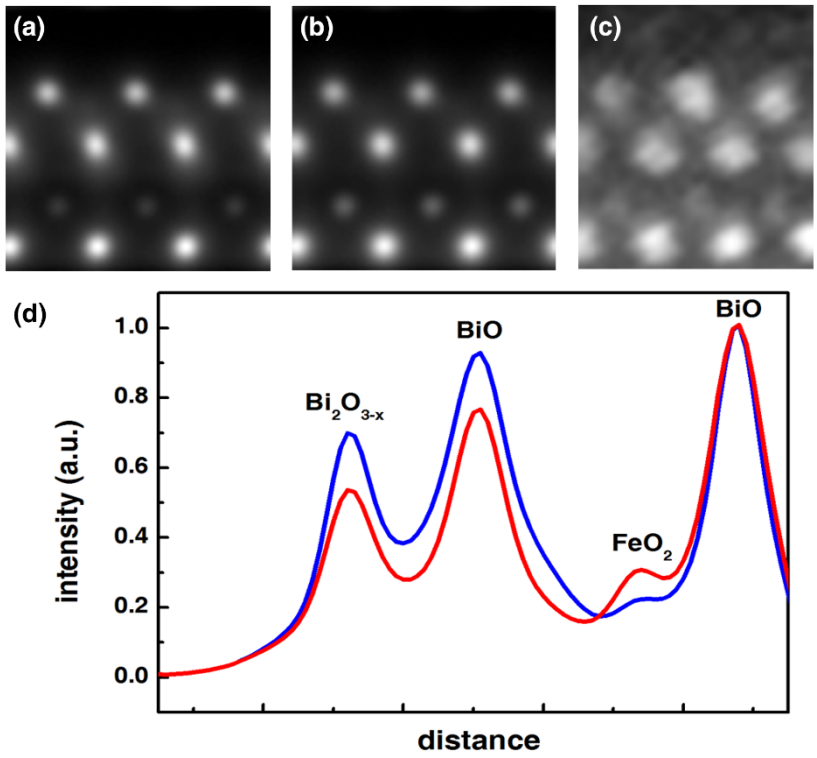

Figure S3. STEM HAADF image simulation results. (a) Simulated image without thermal diffuse scattering. (b) Simulated image with thermal diffuse scattering. (c) Experimental image. (d) Normalized integrated intensity profile along the film's normal direction. The blue and red curves correspond to the calculation results without and with thermal diffuse scatterings, respectively. The contrast of surface monolayer and subsurface BiO layer is substantially reduced with respect to the inner BiO layers due to the island-like structures and surface thermal-vibrations.

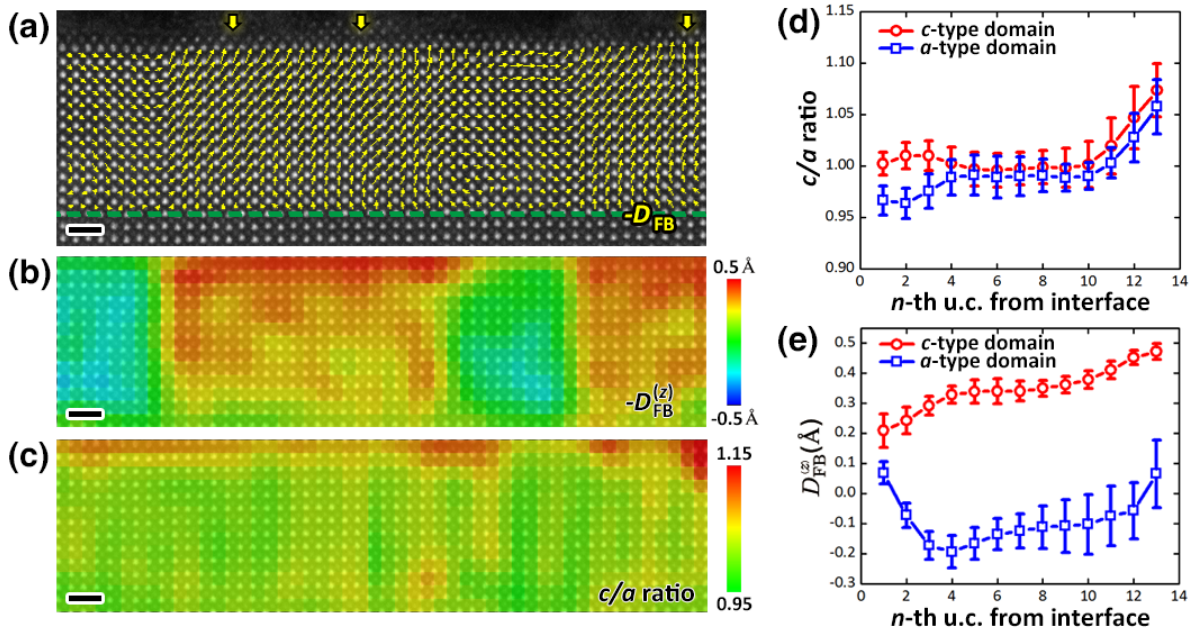

Figure S4. Polarization mapping of 5 nm $BiFeO_3/TbScO_3$ thin film. a) STEM HAADF image and $-\mathbf{D}_{FB}$ mapping of a 5 nm thick $BiFeO_3/TbScO_3$ film viewed along the $[100]_{PC}$ zone axis, where the interface is indicated by the green dashed line. The surface monolayers are indicated by yellow arrows. b) $-D_{FB}^{(z)}$ mapping, c) *c*/*a* ratio mapping of the film. The scalebars in (a)-(c) are 1 nm. d) Quantified *c*/*a* ratio and e) $-D_{FB}^{(z)}$ of *c*-/*a*-type domains.

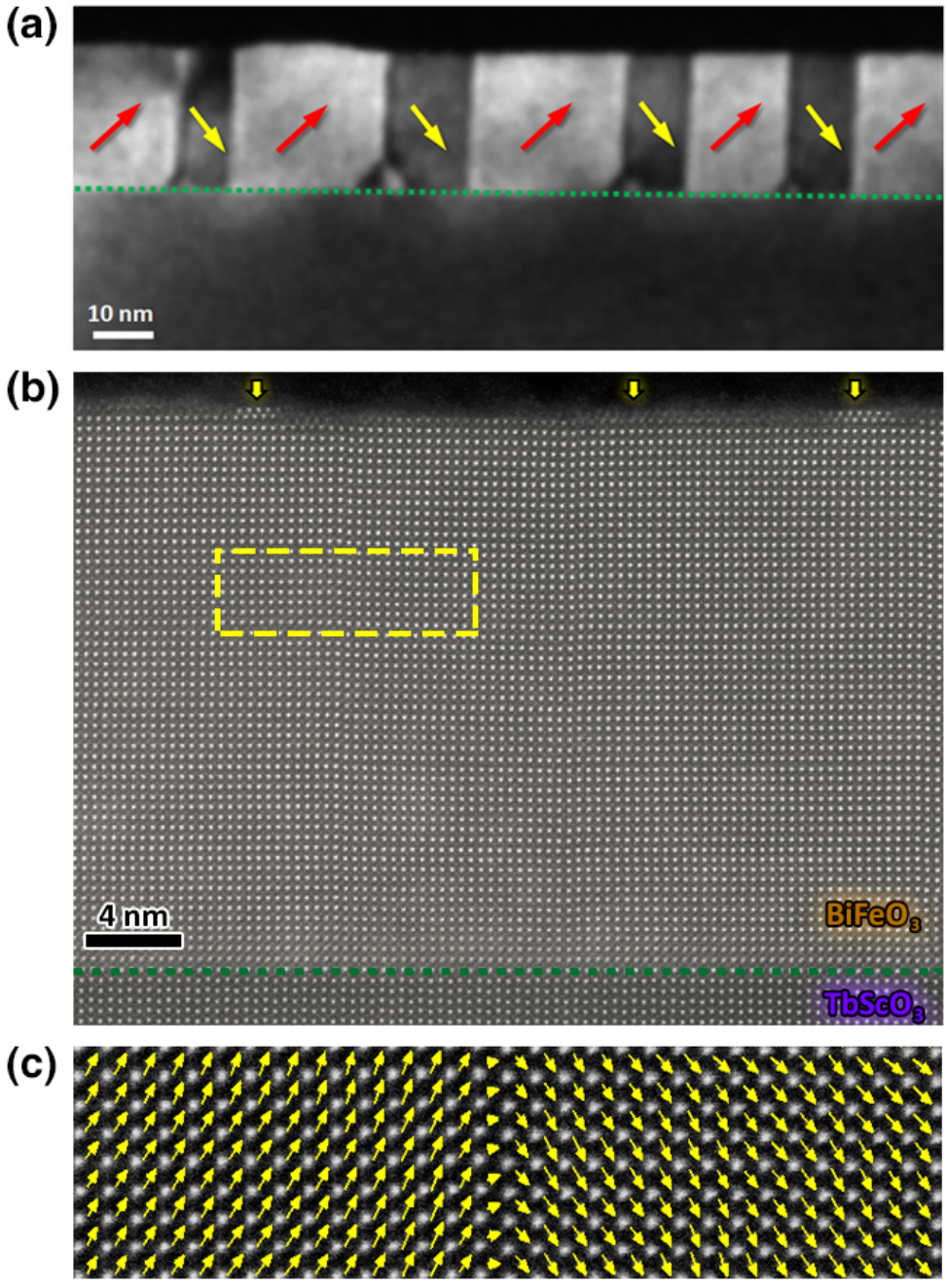

Figure S5. Dark-field and STEM HAADF images of 20 nm $BiFeO_3/TbScO_3$ thin film. a) Dark-field image of a 20 nm thick $BiFeO_3/TbScO_3$ $(1\bar{1}0)_O$ film, in which the interface is indicated by the green dashed line. The red and yellow arrows indicate the polarization of each domain. b) Cross-sectional STEM HAADF image of same film viewed along the $[100]_{PC}$ zone axis; the interface is indicated by the green dashed line. The yellow arrows indicate the surface monolayers. c) $-\mathbf{D}_{FB}$ mapping of the film.

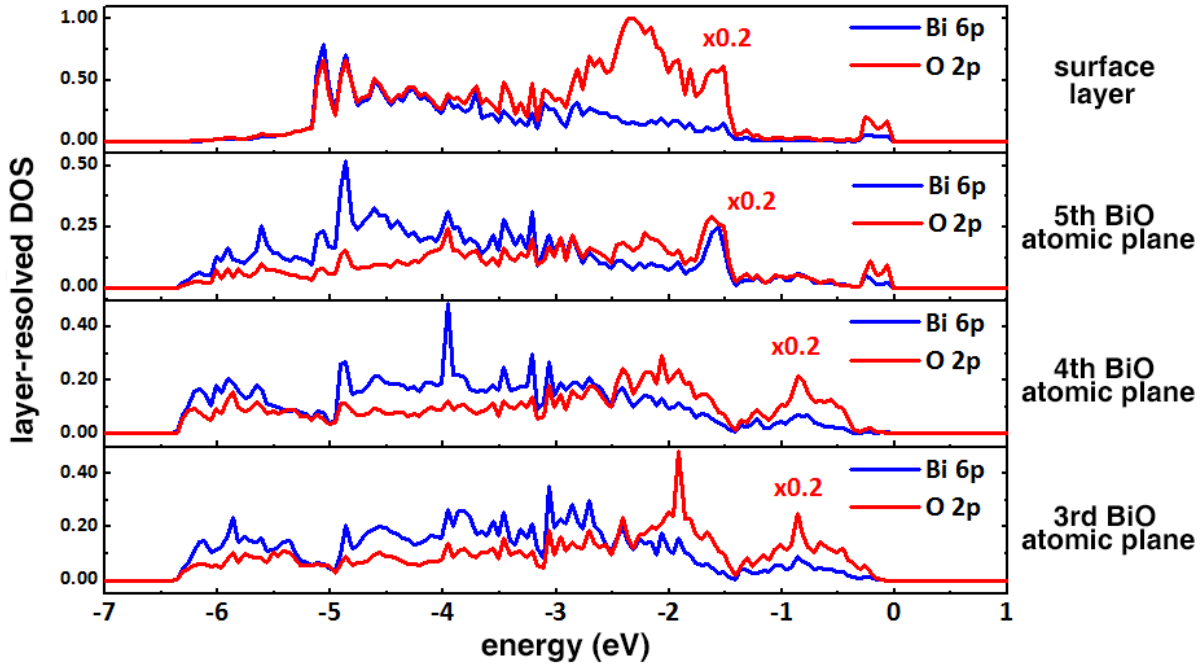

Figure S6. Layer-resolved density of states of Bi 6*p* and O 2*p* electrons in each atomic layer. The Fermi energy is placed at 0 eV and the density of states of O 2*p* electrons is ×0.2 for a better scale. In the surface layer and 5th BiO atomic plane, an overlap of local density of states between Bi 6*p* and O 2*p* orbitals in an energy range from -0.3 eV to 0 eV can be identified.

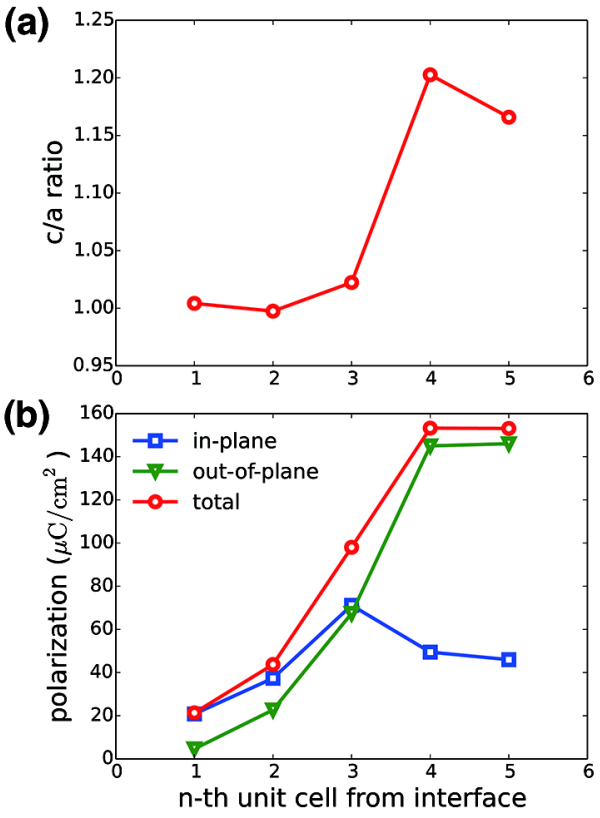

Figure S7. Phase-field simulation results for $BiFeO_3$ film with surface layer. a) *c*/*a* ratio and b) ferroelectric polarization from interface to surface.

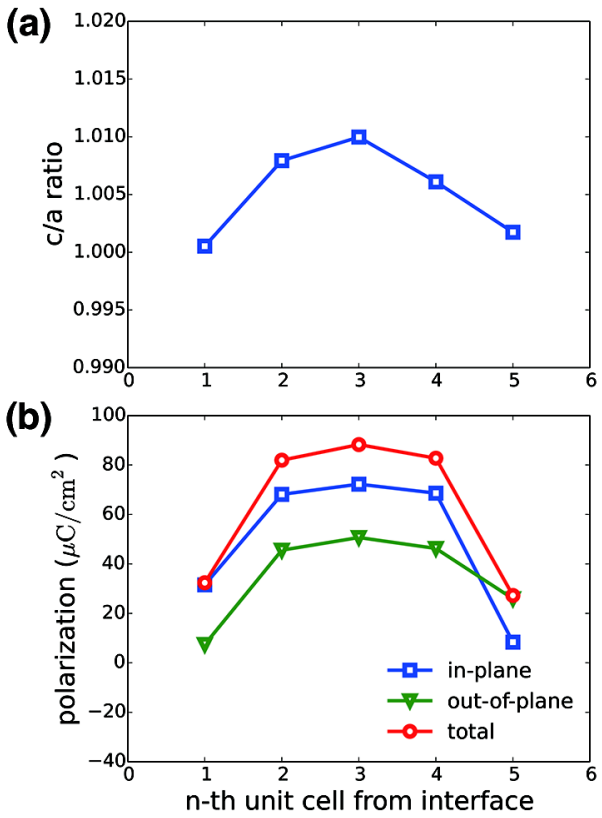

Figure S8. Phase-field simulation results of $BiFeO_3$ film without surface layer. a) *c*/*a* ratio and b) ferroelectric polarization from interface to surface.

	Bi	Fe	O
surface Bi_2O_3 layer	+1.27	-	-1.14
1st BiO layer	+1.64	-	-1.16
1st FeO_2 layer	-	+2.72	-1.18
2nd BiO layer	+1.87	-	-1.20
2nd FeO_2 layer	-	+2.70	-1.19
3rd BiO layer	+1.87	-	-1.19
3rd FeO_2 layer	-	+2.70	-1.19
4th BiO layer	+1.87	-	-1.19
4th FeO_2 layer	-	+2.70	-1.19
5th BiO layer	+1.87	-	-1.19
5th FeO_2 layer	-	+2.70	-1.19

Table S1. Bader charge analysis results of BFO film and surface Bi_2O_3 monolayer. The Bi and O atoms at the surface have relatively lower oxidation state, while the oxidation state of Fe atoms is less affected. Into BFO film, the Bader charge of Bi, Fe and O atoms quickly converges to their bulk values.